

# Bose–Hubbard model for universal quantum walk-based computation

Michael S. Underwood and David L. Feder\*

*Institute for Quantum Information Science, University of Calgary, Alberta T2N 1N4, Canada*

(Dated: October 8, 2018)

We present a novel scheme for universal quantum computation based on spinless interacting bosonic quantum walkers on a piecewise-constant graph, described by the two-dimensional Bose–Hubbard model. Arbitrary  $X$  and  $Z$  rotations are constructed, as well as an entangling two-qubit CPHASE gate and a SWAP gate. Quantum information is encoded in the positions of the walkers on the graph, as in previous quantum walk-based proposals for universal quantum computation, though in contrast to prior schemes this proposal requires a number of vertices only linear in the number of encoded qubits. It allows single-qubit measurements to be performed in a straightforward manner with localized operators, and can make use of existing quantum error correcting codes either directly within the universal gate set provided, or by extending the lattice to a third dimension. We present an intuitive example of a logical encoding to implement the seven-qubit Steane code. Finally, an implementation in terms of ultracold atoms in optical lattices is suggested.

## I. INTRODUCTION

Quantum walks have proven to be a fruitful alternative to the quantum circuit model for the construction and description of quantum information processing tasks [1]. The framework they provide has allowed for the construction of efficient quantum algorithms [2], including some previously unknown under other models [3–8] and alternative formulations of Grover’s search [9] as well as reproductions of other known results [10, 11]. Furthermore, it has since been shown that quantum walks are universal for quantum computation. Three distinct models have been described, based on continuous-time quantum walks [12], discrete-time quantum walks [13], and what we refer to as the discontinuous walk, a hybrid method in which a continuous-time quantum walker takes discrete steps across a set of time-varying graphs, undergoing perfect state transfer through a subset of the graph at each stage [14]. In each case, the use of a single walker to encode  $n$  qubits leads to a graph with  $\Omega(2^n)$  vertices.

One straightforward adaptation that allows for the exponentially growing Hilbert space required to encode  $n$  qubits without necessitating a similarly sized graph is to employ multiple quantum walkers. As a step in that direction, a framework for the description of multiple non-interacting discrete-time quantum walkers, distinguishable or not, has been put forth [15]. It is straightforward to see though that if there are multiple walkers on a graph yet they do not interact, then there is no meaningful difference from the situation of multiple distinct copies of the single-walker situation. Non-interacting walkers evolve independently of each other, so while they can be useful if many runs are required to build up statistics of the output state, no new dynamics can be present.

In the discrete-time quantum walk, effective interactions between otherwise non-interacting walkers can be

induced through the sharing or swapping of coins [16], and entanglement can arise between a single walker and its coin [17]. Continuous-time quantum walks on the other hand have no coin degree of freedom, so must rely on inter-walker interactions to introduce additional dynamics and generate entanglement. There is evidence that on a given graph, two interacting continuous-time walkers are more computationally powerful than either a single walker or two non-interacting ones when applied to the graph isomorphism problem [18].

For the case of the continuous-time quantum walk, the Bose–Hubbard model [19] provides a natural method with which to describe interacting bosonic walkers, and its relationship to a single continuous-time quantum walker has been discussed in the context of particle transport and entanglement generation [20]. The model is well studied in the realm of condensed-matter physics; in particular it describes strongly correlated systems well [21], providing an excellent description of features such as the transition between the superfluid and Mott-insulator phases, as well as having been implemented and well controlled experimentally [22]. Furthermore the standard Bose–Hubbard Hamiltonian does not address internal degrees of freedom, allowing us to explicitly consider the encoding of quantum information within position states, in the spirit of quantum walks, rather than a more conventional encoding in spin states.

Standard quantum walk-based schemes for quantum computation employ a position-based encoding. This results in a spatially delocalized qubit under circumstances where the quantum walk formalism can be directly mapped to the circuit model. In this work, we assign a pair of vertices to each bosonic walker, corresponding directly to the computational states  $|0\rangle$  and  $|1\rangle$ . Gates are implemented by making instantaneous changes to the graph supporting the walkers, and we explicitly require couplings to doubly occupied states in which two walkers interact on one vertex, despite the fact that such states do not encode qubits. The graph is fixed except at the instants of change, so continuous dynamical control is not required. The main idea is to design a discrete

---

\* Corresponding author: dfeder@ucalgary.ca

sequence of graphs, such that at the beginning and end, the spatial separation of the walkers is maintained with one walker per pair of vertices, yet during their evolution the walkers have the opportunity to interact whenever two walkers occupy one vertex. This allows states with doubly occupied vertices to be harnessed as an advantage in constructing logical gates, rather than having to be strictly avoided as a source of decoherence during gate operations as in previous proposals [23].

In this work we provide an important correspondence between the discontinuous evolution of interacting indistinguishable particles on polynomial-sized graphs and that of a single discontinuous quantum walker on an exponentially larger graph. That is, a number of walkers linear in the number of qubits to be simulated  $n$ , walking on a vertex set of a size also linear in  $n$ , has the same power as a quantum walk with a constant number of walkers (in particular, one walker) on a graph with a number of vertices exponential in  $n$ .

The structure of this article is as follows. In Sec. II we briefly review the Bose–Hubbard Hamiltonian, then define an encoding of computational basis states within a subset of the position states available to the bosons in the system it governs, and describe a set of physical operations that result in a universal set of one- and two-qubit gates on the computational space. We then describe in Sec. III how single-qubit measurements can be made on encoded qubits, and provide an example scheme for adding a layer of quantum error correction. Finally in Sec. IV we discuss the possibility of a proof-of-concept implementation of our scheme, before providing some concluding remarks in Sec. V.

## II. POSITIONS AS COMPUTATIONAL STATES

### A. The Bose–Hubbard Hamiltonian

We use the Bose–Hubbard model to describe multiple interacting continuous-time quantum walkers on a graph as spinless bosons hopping on a lattice, with on-site interactions. The graph  $G$  is defined by a set of vertices  $V$  and associated edges  $E \subseteq V \times V$ . The vertices correspond to the lattice sites, while the edges indicate allowed tunnelings. The Bose–Hubbard Hamiltonian is

$$\hat{\mathcal{H}} = -J \sum_{\langle i,j \rangle} \hat{c}_i^\dagger \hat{c}_j + \frac{U}{2} \sum_i \hat{n}_i (\hat{n}_i - 1). \quad (1)$$

Here  $\hat{c}_i^\dagger$  creates a particle on vertex  $i$  and  $n_i \equiv \hat{c}_i^\dagger \hat{c}_i$  is the number operator on said vertex. The first sum runs over neighboring vertices  $\langle i,j \rangle$  such that  $(i,j) \in E$  is an edge of the lattice graph.  $J$  is the tunneling amplitude between adjacent sites, and  $U$  is the on-site interaction strength between the particles.

We refer to the graph  $G$ , on which multiple quantum walkers appear, as the *primary* graph. This primary

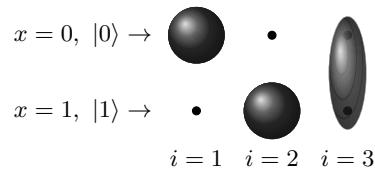


FIG. 1. Cartoon representation of six vertices confining  $n = 3$  particles whose positions encode a computational state of the form  $|\psi\rangle = |0\rangle \otimes |1\rangle \otimes |+\rangle$ . The physical Hilbert space  $\mathbf{H}$  for this setup is 56-dimensional. The Hamiltonians we prescribe couple the encoded 8-dimensional computational space  $\mathbf{C}$  to a total of 24 of the 56 basis states.

graph and the  $n$  walkers evolving on it comprise a physical system that can be described by a set of states and allowed transitions between pairs of them. One can consider each of these states as corresponding with a vertex in a *secondary* graph, in which each allowed transition appears as an edge. The evolution of  $n$  walkers on the primary graph then maps exactly onto the evolution of a single walker on the secondary graph. Note that the number of vertices in the secondary graph is at least exponentially larger than the number of vertices in  $G$ .

We make use of  $n$  bosonic quantum walkers to encode  $n$  qubits. On a primary graph of  $2n$  vertices we assign a pair of vertices to each qubit, and for simplicity visualize the vertices as being arranged in a  $2 \times n$  grid structure; see Fig. 1 for a cartoon example with  $n = 3$ . Label the vertices  $v_{i,x} \in V$ , with  $i \in \{1, \dots, n\}$  and  $x \in \{0, 1\}$ , and let  $|0_{i,x}\rangle$  be the vacuum state on vertex  $v_{i,x}$  in row  $x$  of column  $i$ . The vacuum state of the system is then

$$|\text{vac}\rangle = |0_{1,0}0_{1,1} \cdots 0_{n,0}0_{n,1}\rangle, \quad (2)$$

which when convenient can also be expressed as

$$|\text{vac}\rangle = |00\rangle_1 \cdots |00\rangle_n, \quad (3)$$

where the first (second) entry in each pair is understood to correspond with row 0 (1) of the array. A walker is created on vertex  $v_{i,x}$  by the operator  $\hat{c}_{i,x}^\dagger$ .

The physical Hilbert space  $\mathbf{H}$  of  $n$  bosons confined to such a lattice is larger than the  $2^n$ -dimensional computational Hilbert space  $\mathbf{C}$  which their positions encode. The encoding is accomplished with a subset  $\mathbf{H}_{\mathbf{C}} \subset \mathbf{H}$ , such that  $|\mathbf{H}_{\mathbf{C}}| = 2^n$ , along with an isomorphism  $\text{ENC} : \mathbf{H}_{\mathbf{C}} \rightarrow \mathbf{C}$ . Generally we can use  $\mathbf{C}$  and  $\mathbf{H}_{\mathbf{C}}$  interchangeably without ambiguity. In order to generate entangled states in  $\mathbf{C}$  we make use of a Hamiltonian that couples  $\mathbf{H}_{\mathbf{C}}$  to states outside of the computational space, i.e. those in  $\mathbf{H}_{\perp} \equiv \mathbf{H} \setminus \mathbf{H}_{\mathbf{C}}$ . Under our scheme, a physical state  $|\Psi\rangle \in \mathbf{H}_{\mathbf{C}}$  provides a valid encoding of a computational state on  $n$  qubits,  $|\Psi\rangle_{\mathbf{C}} = \text{ENC}(|\Psi\rangle)$ , while any state  $|\alpha\rangle \in \mathbf{H}$  that has non-zero support in  $\mathbf{H}_{\perp}$  has no such encoding. Since the computationally entangling Hamiltonian couples  $\mathbf{H}_{\mathbf{C}}$  to  $\mathbf{H}_{\perp}$ , the evolution of the system restricted to  $\mathbf{C}$  appears to be non-unitary in that the magnitude of the projection of the physical state of the

system onto the subspace  $\mathbf{H}_C$  can be different from unity. However, we show that an arbitrary initial state with support entirely in  $\mathbf{H}_C$  will, at well-defined times in its evolution under the Hamiltonians we specify, map onto a state that also has no support in  $\mathbf{H}_\perp$ . That is, all probability will return to  $\mathbf{C}$  and the physical system will once again encode a valid computational state.

The ability to construct an entangling Hamiltonian under this encoding relies on the indistinguishability of the bosons involved as the encoding we use requires the operations of interchanging two particles on the lattice and of swapping them twice, returning them to their initial configuration, to be identical. This is crucial for preserving the mapping from the physical system to the computational space that requires one bosonic walker to be localized to two vertices of the primary graph.

We assume that unless an explicit operation is being performed, the lattice is deep enough to prevent all tunneling. In this default configuration the system Hamiltonian is

$$\hat{\mathcal{H}}_0 = \frac{U}{2} \sum_{i=1}^n \sum_{x=0}^1 \hat{n}_{i,x} (\hat{n}_{i,x} - 1). \quad (4)$$

This results in a primary graph that is completely disconnected —  $2n$  vertices with no edges,  $E = \emptyset$ . Each two-site column of the lattice represents a qubit, with the upper and lower sites corresponding to the  $|\underline{0}\rangle$  and  $|\underline{1}\rangle$  computational basis states of that qubit, respectively. An  $n$ -particle state  $|\Psi\rangle$  represents a valid computational state if and only if

$$\sum_{x=0}^1 \left| \langle \Psi | \hat{c}_{i,x}^\dagger \hat{c}_{i,x} | \Psi \rangle \right|^2 = 1 \quad (5)$$

for each  $i$  from 1 to  $n$ , i.e. if there is one particle in each column. Physical states that satisfy this criterion are mapped onto computational ones in a canonical way,

$$|\underline{0}\rangle_i \leftrightarrow \hat{c}_{i,0}^\dagger |00\rangle_i = |10\rangle_i, \quad (6a)$$

$$\text{and } |\underline{1}\rangle_i \leftrightarrow \hat{c}_{i,1}^\dagger |00\rangle_i = |01\rangle_i. \quad (6b)$$

We use underlines to indicate encoded computational states, in contrast with physical Fock-number states. The system is initialized in the state

$$|\Psi_0\rangle = \bigotimes_{i=1}^n \hat{c}_{i,0}^\dagger |\text{vac}\rangle \leftrightarrow |\underline{0}\rangle^{\otimes n}. \quad (7)$$

This is a zero-energy eigenstate of  $\hat{\mathcal{H}}_0$ , and as such is stationary while the lattice is maintained and the primary graph has no edges.

The dimension of  $\mathbf{H}$  is  $\binom{2n}{n}$ , in general much larger than  $|\mathbf{C}| = 2^n$ . This may seem inefficient or even detrimental at first sight, but it is this access to a larger Hilbert space during evolution that allows for the implementation of a two-qubit controlled gate through only on-site

interactions with no internal degrees of freedom. We impose Hamiltonians that couple  $\mathbf{H}_C$  to  $\mathbf{H}_\perp$  in such a way that at well-defined times the resulting unitary operators block diagonalize as  $\hat{U} = \hat{U}_C \oplus \hat{U}_\perp$ . That is, all population initially in a valid computational state returns to the computational subspace at the end of the evolution, despite having been transferred through the larger space at intermediate times.

Before discussing our two-qubit gates, in particular an entangling CPHASE gate and a nearest-neighbor SWAP, we first provide a simple method for implementing arbitrary single-qubit operations.

## B. Single-qubit operations

Consider the  $i$ th encoded qubit, with computational basis states  $|\underline{0}\rangle_i$  and  $|\underline{1}\rangle_i$  encoded according to (6) in a physical state  $|\Psi\rangle$  satisfying the single-particle condition (5). The single-qubit operations we construct below trivially preserve this condition, as they do not couple  $|\Psi\rangle$  to states outside of the computational space.

We first show how to implement an arbitrary  $X$  rotation on qubit  $i$ . By lowering the height of the lattice barrier between the two sites we can set the system Hamiltonian to

$$\hat{\mathcal{H}}_{X,i} = -J_{X,i} \left( \hat{c}_{i,0}^\dagger \hat{c}_{i,1} + \text{H.c.} \right) + \hat{\mathcal{H}}_0, \quad (8)$$

where  $J_{X,i}$  depends on the height of the lowered barrier between the sites. The primary graph in this case is composed of  $2(n-1)$  disconnected vertices and one copy of  $K_2$ , the connected two-vertex graph, on the vertices encoding qubit  $i$ . The action of  $\hat{\mathcal{H}}_{X,i}$  on the basis states (6) is simply

$$\hat{\mathcal{H}}_{X,i} : |10\rangle_j \mapsto -\delta_{ij} J_{X,i} |01\rangle_j, \quad (9a)$$

$$|01\rangle_j \mapsto -\delta_{ij} J_{X,i} |10\rangle_j, \quad (9b)$$

where  $\delta_{ij}$  is the Kronecker delta. In the computational space this acts as an  $X$  operator on qubit  $i$ ,

$$\hat{\mathcal{H}}_{X,i} : |\underline{0}\rangle_i \mapsto -J_{X,i} |\underline{1}\rangle_i, \quad (10)$$

$$|\underline{1}\rangle_i \mapsto -J_{X,i} |\underline{0}\rangle_i, \quad (11)$$

and does nothing to the other qubits encoded in  $|\Psi\rangle$ . The unitary operator generated by evolution under this Hamiltonian for a time  $t$  is then  $\hat{U}_{X,i}(t) = \hat{R}_{X,i}(-2J_{X,i}t)$ , an  $X$  rotation of the  $i$ th qubit.

Next we construct a  $Z$  rotation on qubit  $i$ . To do so, we maintain the initial height of the barrier between the two sites while applying a local potential to the  $|\underline{1}\rangle_i$  site. The physical Hamiltonian becomes

$$\hat{\mathcal{H}}_{Z,i} = -V_{Z,i} \hat{n}_{i,1} + \hat{\mathcal{H}}_0 \quad (12)$$

and corresponds to a primary graph of  $2n$  disconnected vertices, with a self-loop attached to the second of the

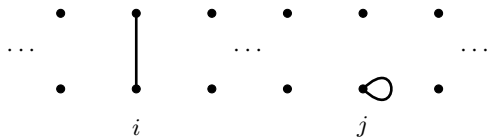


FIG. 2. An  $n$ -walker graph on  $2n$  vertices, on which appropriately initialized bosonic walkers will undergo  $X$  and  $Z$  rotations on the encoded qubits  $i$  and  $j$ , respectively.

two vertices that encode qubit  $i$ . The Hamiltonian acts only on the  $|\underline{1}\rangle_i$  computational basis state, as

$$\hat{\mathcal{H}}_{Z,i} : |\underline{1}\rangle_j \mapsto -\delta_{ij} V_{Z,i} |\underline{1}\rangle_j, \quad (13)$$

so the resulting unitary is  $\hat{U}_{Z,i}(t) = e^{iV_{Z,i}t/2} \hat{R}_{Z,i}(V_{Z,i}t)$  — a  $Z$  rotation of qubit  $i$ , up to an unimportant overall phase.

Given an angle  $\theta \in [0, 2\pi)$  we can therefore perform  $\hat{R}_X(\theta)$  on qubit  $i$  by evolving under  $\hat{\mathcal{H}}_{X,i}$  for a time

$$t_{X,i}(\theta) = \frac{4\pi - \theta}{2J_{X,i}}, \quad (14a)$$

or  $e^{i\theta/2} \hat{R}_Z(\theta)$  by evolving under  $\hat{\mathcal{H}}_{Z,i}$  for a time

$$t_{Z,i}(\theta) = \frac{\theta}{V_{Z,i}}. \quad (14b)$$

Given sufficient freedom in the ability to set the tunneling rates and on-site potentials, it is possible to enact either of these single-qubit gates on each qubit simultaneously, with different values of  $\theta$  on each one, and have them finish at the same time. That is, given a set of angles  $\theta_i$  and a choice of gates  $\hat{O}_i \in \{\hat{R}_X, \hat{R}_Z, \hat{I}\}$ , the values of  $J_{X,i}$  and  $V_{Z,i}$  can be chosen such that in a fixed time  $t$ , the operations  $\hat{O}_i(\theta_i)$  are simultaneously applied across all qubits  $i \in \{1, \dots, n\}$ . Fig. 2 shows an example multi-walker primary graph that applies an  $X$  rotation to qubit  $i$  and a  $Z$  rotation to qubit  $j$ . The combination of these operations allows for the execution of arbitrary single-qubit unitaries in three steps by decomposing the corresponding rotations of the Bloch sphere using Euler angles.

Finally, we note that while these single-qubit operators are sufficient to implement a Hadamard operation on qubit  $i$  in three steps, as

$$\hat{H}_i = \hat{R}_{X,i}(\pi/2) \hat{R}_{Z,i}(\pi/2) \hat{R}_{X,i}(\pi/2), \quad (15)$$

it is also possible to obtain a Hadamard in a single step with the Hamiltonian

$$\hat{\mathcal{H}}_{H,i} = -V_{H,i} \hat{n}_{i,0} - J_{H,i} (\hat{c}_{i,0}^\dagger \hat{c}_{i,1} + \text{H.c.}) + \hat{\mathcal{H}}_0. \quad (16)$$

This simple approach of effectively turning on the Hamiltonians for  $X$  and  $Z$  rotations simultaneously results in the application of a Hadamard gate on qubit  $i$ , up to an overall phase, at time

$$t_{H,i} = \frac{\pi}{2\sqrt{2}J_{H,i}} \quad (17)$$

if the applied-potential-to-hopping ratio is tuned to be  $V_{H,i}/J_{H,i} = 2$ . Not only does this one-step process require fewer dynamical controls, but for equal hopping and interactions terms (i.e. taking  $J_{H,i} = J_{X,i}$  and  $V_{Z,i} = V_{H,i}$ ) results in a run-time that is an order of magnitude shorter. This example is unlikely to be the only such shortcut to additional gates available by judicious choices of further Hamiltonians.

### C. Generating entanglement

We now show how to generate entanglement between adjacent qubits, in the form of a controlled phase gate,  $\text{CPHASE}(\phi)$ . We must expand our discussion to a  $2 \times 2$  contiguous sub-block of the entire lattice, which we take to be the vertices  $v_{i,x}$  and  $v_{i+1,x}$ , for  $x \in \{0, 1\}$ , and we again assume that the initial  $n$ -qubit state  $|\Psi\rangle$  satisfies condition (5), containing one bosonic walker per two-site column. Restricting our attention to two walkers on four sites, the physical space in question is 10 dimensional. Four basis states correspond to the computational basis, and we will couple these to an additional four physical states. The remaining two physical basis states can be ignored so long as the initial state is a computational one. For convenience we drop subscripts and write the Fock states on the four vertices in question as a single ket when there is no ambiguity from doing so, taking for example  $|0110\rangle = |01\rangle_i |10\rangle_{i+1}$ . The two-qubit computational space is encoded in the Fock number states

$$\hat{c}_{i,0}^\dagger \hat{c}_{i+1,0}^\dagger |0000\rangle = |1010\rangle \leftrightarrow |\underline{00}\rangle, \quad (18a)$$

$$\hat{c}_{i,0}^\dagger \hat{c}_{i+1,1}^\dagger |0000\rangle = |1001\rangle \leftrightarrow |\underline{01}\rangle, \quad (18b)$$

$$\hat{c}_{i,1}^\dagger \hat{c}_{i+1,0}^\dagger |0000\rangle = |0110\rangle \leftrightarrow |\underline{10}\rangle, \quad (18c)$$

$$\hat{c}_{i,1}^\dagger \hat{c}_{i+1,1}^\dagger |0000\rangle = |0011\rangle \leftrightarrow |\underline{11}\rangle. \quad (18d)$$

The six physical basis states  $|1100\rangle$ ,  $|0011\rangle$ ,  $|2000\rangle$ ,  $|0200\rangle$ ,  $|0020\rangle$ , and  $|0002\rangle$  have no computational interpretation. We can think about the two-qubit situation in two complementary ways. The first is as we have described, a four-vertex primary graph on which there are two interacting quantum walkers. The second is to treat each of the physical basis states as a vertex in a new single-walker secondary graph on 10 vertices, with edges prescribed by the transitions allowed under the Hamiltonian in question. For example, the physical and computational bases under the Hamiltonian we will introduce for generating entanglement are represented in Fig. 3, with the primary graph in (a) and the corresponding secondary graph in (b).

To implement a  $\text{CPHASE}$  gate, we decrease the barrier height between the sites corresponding to  $|\underline{1}\rangle_i$  and  $|\underline{1}\rangle_{i+1}$  so that the system Hamiltonian is

$$\hat{\mathcal{H}}_{\text{CP},i} = -J_{\text{CP}} (\hat{c}_{i,1}^\dagger \hat{c}_{i+1,1} + \text{H.c.}) + \hat{\mathcal{H}}_0. \quad (19)$$

Let  $\hat{U}_{\text{CP}}(t) \equiv \exp(-i\hat{\mathcal{H}}_{\text{CP}}t)$  be the time-evolution operator

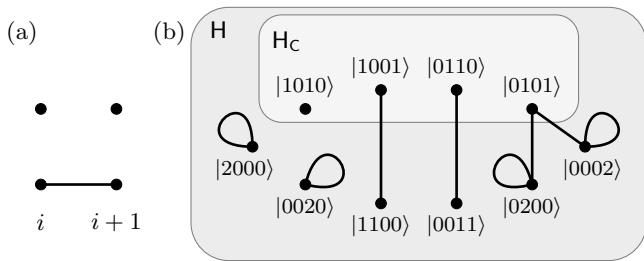


FIG. 3. (a) The primary two-walker subgraph on which encoded qubits  $i$  and  $i+1$  undergo a CPHASE operation has four vertices and a single edge. (b) The corresponding secondary graph, describing the couplings among Fock states under the Hamiltonian  $H_{CP}$ , in columns  $i$  and  $i+1$  of the physical graph, has 10 vertices to represent the 10-dimensional Fock space  $H$  of two bosons on four sites. Four of these are selected to encode the computational space  $H_C$ . Edges between vertices correspond to allowed transitions, and self loops to on-site interactions.

generated by  $\hat{\mathcal{H}}_{CP}$ , where we have dropped the ‘ $i$ ’ subscripts when no ambiguity arises from doing so. Then for any time  $t$ , the  $|00\rangle$  computational state evolves as  $\hat{U}_{CP}(t)|1100\rangle = |1100\rangle$ . The state encoding  $|01\rangle$  couples outside of the computational basis, to  $|1100\rangle$ ; at time  $t$ ,

$$\hat{U}_{CP}(t)|1001\rangle = \cos(J_{CP}t)|1001\rangle + i \sin(J_{CP}t)|1100\rangle. \quad (20)$$

In order to guarantee that  $\hat{U}_{CP}$  maps computational states to computational states, we must therefore require it to act for a time  $t_{CP,k} \equiv k\pi/J_{CP}$ ,  $0 < k \in \mathbb{Z}$ . This also satisfies the requirement that  $|10\rangle$  be mapped to the computational basis. Specifically, for  $|\psi\rangle \in \{|1001\rangle, |0110\rangle\}$  we have  $\hat{U}_{CP}(t_{CP,k})|\psi\rangle = (-1)^k|\psi\rangle$ .

The fourth computational state on two qubits,  $|11\rangle$ , evolves within a three-dimensional subspace spanned by  $|0101\rangle$ ,  $|0200\rangle$ , and  $|0002\rangle$ , as illustrated by the largest connected component of the secondary graph in Fig. 3(b). Determining the action of  $\hat{U}_{CP}$  on  $|0101\rangle$  shows that for a walker initially in this state to return entirely to the computational basis at time  $t_{CP,k}$  requires

$$\exp\left[2\pi i \sqrt{16 + \frac{U^2}{J_{CP}^2}}\right] = 1. \quad (21)$$

This is accomplished if the ratio of the on-site repulsion to the hopping rate is tuned to be  $U/J_{CP} = \sqrt{m^2 - 16}$ , for any integer  $m \geq 4$ . The final requirement to guarantee that  $U_{CP}$  maps the computational space onto itself at time  $t_{CP,k}$  is that the product  $mk$  be even. We can guarantee this by setting  $k = 2$ , defining  $t_{CP} = 2\pi/J_{CP}$ . In this case the action of  $\hat{U}_{CP}$  decomposes into its action on the computational basis states, and its action on the rest of Fock space. In the canonical ordering of the computational basis states, we have

$$\hat{U}_{CP}(t_{CP}) = \text{diag}\left(1, 1, 1, e^{-i\pi(m+\sqrt{m^2-16})}\right) \oplus \hat{U}_{CP}^\perp \quad (22a)$$

$$= \text{CPHASE}(\varphi_m) \oplus \hat{U}_{CP}^\perp, \quad (22b)$$

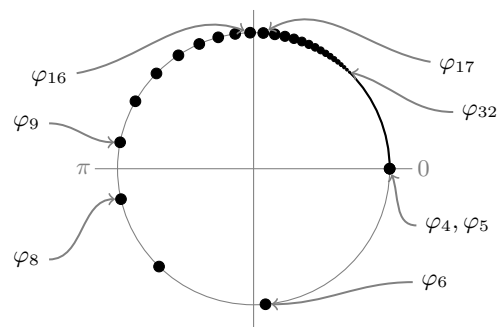


FIG. 4. Distribution of available phases  $\varphi_m$  satisfying (23). Except for the two trivial values,  $\varphi_4$  and  $\varphi_5$ , no phase is a rational multiple of  $\pi$ . For large  $m$  the phase goes as  $-8\pi/m$ , modulo  $2\pi$ , returning to 0 as  $m \rightarrow \infty$ , which corresponds to the limit of zero hopping.

where  $\hat{U}_{CP}^\perp$  acts only on the subspace orthogonal to the computational one, and

$$\varphi_m \equiv -\pi \left(m + \sqrt{m^2 - 16}\right). \quad (23)$$

This is a non-trivial entangling phase for any  $m > 5$ , and the available values are depicted graphically on the unit circle in Fig. 4.

If we instead choose an odd value for  $k$ , including  $k = 1$  which results in a shorter run-time for the gate, the even values of  $m \geq 4$  result in the same set of phases but indexed by  $m/2$  rather than  $m$ . The resulting gate in this case is  $(Z \otimes Z)\text{CPHASE}(\varphi_{m/2})$ .

#### D. SWAP gate

In order to provide a universal gate set with only a nearest-neighbor entangling gate, a two-qubit SWAP gate is also required. A variation of the  $X$  rotation performed by  $\hat{\mathcal{H}}_{X,i}$  allows for a straightforward implementation of this by the simultaneous lowering of the potential barrier between sites  $|\underline{x}\rangle_i$  and  $|\underline{x}\rangle_{i+1}$ , for each  $x \in \{0, 1\}$ . The system Hamiltonian in this case is

$$\hat{\mathcal{H}}_{S,i} = -J_S \left(c_{i,0}^\dagger c_{i+1,0} + c_{i,1}^\dagger c_{i+1,1} + \text{H.c.}\right) + \hat{\mathcal{H}}_0. \quad (24)$$

This acts non-trivially on the four basis states satisfying (5), coupling the computational space to all six of the remaining physical basis states. As with the analysis of the CPHASE gate, we can place restrictions on the available parameters such that the action of the operation restricted to the computational space is unitary at the end of the evolution. The action of  $\hat{\mathcal{H}}_S$  on  $|1001\rangle$  and  $|0110\rangle$  requires that we set the SWAP time to be

$$t_{S,k} = \frac{(2k+1)\pi}{2J_S}, \quad 0 \leq k \in \mathbb{Z}. \quad (25a)$$

Under this restriction, the action of  $\hat{\mathcal{H}}_S$  on  $|1010\rangle$  and  $|0101\rangle$  further requires that

$$\frac{U}{J_S} = 4\sqrt{\frac{l^2}{(2k+1)^2} - 1}, \quad 2k+1 < l \in \mathbb{Z}. \quad (25b)$$

When these conditions are satisfied, the action of  $\hat{U}_S(t) \equiv \exp(-i\hat{\mathcal{H}}_S t)$  at time  $t = t_{S,k}$  block diagonalizes such that its effect on the computational space is that of

$$\hat{U}_S(t_{S,k})\Big|_{\text{Hc}} = \begin{pmatrix} e^{-i\alpha\pi} & 0 & 0 & 0 \\ 0 & 0 & -1 & 0 \\ 0 & -1 & 0 & 0 \\ 0 & 0 & 0 & e^{-i\alpha\pi} \end{pmatrix} \quad (26)$$

with

$$\alpha = l + \sqrt{l^2 - 4k(k+1)} - 1. \quad (27)$$

In general this provides us with a second entangling gate, unless  $\alpha$  is an integer. In that case, if  $\alpha$  is even then (26) is equivalent to  $(Z \otimes Z)\text{SWAP}$ , and if it is odd then we obtain the gate  $-\text{SWAP}$ .

The problem of finding values for  $k$  and  $l$  that satisfy the conditions (25) while resulting in an integral value of  $\alpha$  reduces to finding Pythagorean triples, of which there are infinitely many. One such combination, which results in the minimal time for the operation, is  $k = 1$  and  $l = 5$ . This pair leads to the parameters  $t_S = 3\pi/(2J_S)$  and  $U/J_S = 16/3$ , and implements a two-qubit nearest-neighbor SWAP gate, up to an overall phase, as required for a universal gate set.

### E. Connection to discontinuous walks

Implementing a sequence of computational gates requires that we toggle a set of potentials on and off in a prescribed order, affecting the evolution of a set of quantum walkers in the process. This is in the same spirit as the single-walker discontinuous walk we have previously proposed [14], though that work makes use of a number of vertices exponential in the number of encoded qubits whereas in the current multi-walker scheme only linear growth is required in the number of vertices.

As in the prior models of universal computation by quantum walk [12, 13], the single-walker discontinuous model employs a set of ‘rails’ for encoding the quantum information. These rails are linear graphs that allow propagation of information from left to right, interspersed with so-called ‘widgets’ that enact transformations on the state of the walker as it passes them. There is one rail for each computational basis state, which leads to the exponential growth in vertices. In Fig. 5 we show how a time sequence of two-walker primary graphs on four vertices corresponds to a single discontinuous walker on a larger secondary graph, and draw a connection to the rail model. Since  $2n = 2^n$  for  $n = 2$  the number

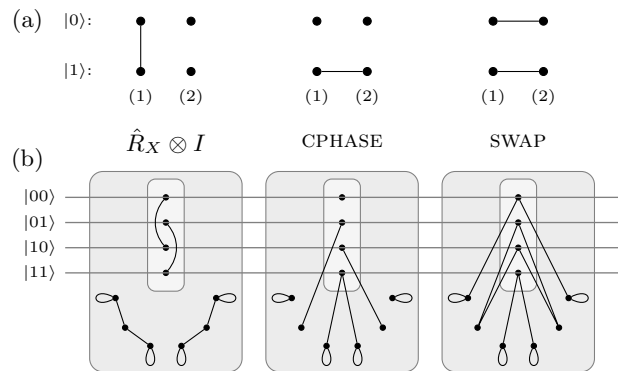


FIG. 5. (a) Hopping parameters turned on to enact gates with two qubits present. (b) The corresponding graphs encoding couplings among the ten states of  $\text{H}$  are presented in gray for each operation, with the four computational states of  $\text{Hc}$  highlighted in light gray.

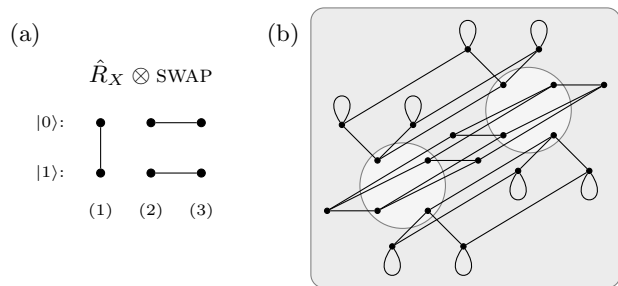


FIG. 6. When three qubits are encoded, (a) three edges among the six vertices of the primary graph implement an  $\hat{R}_X \otimes \text{SWAP}$  gate. (b) The corresponding secondary graph is much larger, and is given by the cartesian product of the one- and two-qubit graphs for  $\hat{R}_X$  and SWAP. Note that those vertices which are not connected to the computational states have been omitted in an attempt at clarity.

of rails is equal to the number of vertices in this case, though in Fig. 6 we show what a single step of a discontinuous walk on three qubits looks like, on six vertices in the primary multi-walker case and on eight rails in a 56-dimensional space for a single walker on the resulting secondary graph.

### III. MEASUREMENTS AND ERROR CORRECTION

Under a single-walker model for computation, a measurement of the computational states of  $m \leq n$  qubits can be accomplished either in a single step with a set of  $\Omega(2^m)$  physical measurement operators, each spatially delocalized over  $\Omega(2^{n-m})$  vertices, or as a sequence of  $m$  single-qubit measurements, each requiring two measurement operators delocalized over  $\Omega(2^{n-1})$  vertices. Assume the best-case scenario of there being a one-to-one mapping between the computational basis states and a (sub)set of  $2^n$  vertices. For  $x \in \{0, \dots, 2^m - 1\}$ , let

$x = x_1 \cdots x_m$  be the  $m$ -bit binary expansion of  $x$ . To make a measurement of qubits  $\{i_k\}_{k=1}^m$ , let  $\mathcal{V}_x$  be the set of integers between 0 and  $2^n - 1$  whose  $n$ -bit binary expansions have bit value  $x_k$  at bit position  $i_k$ . Then the measurement operators required are

$$\left\{ P_x = \sum_{v \in \mathcal{V}_x} |v\rangle\langle v| \right\}_{x=0}^{2^m-1}. \quad (28)$$

Clearly there are  $2^m$  values of  $x$ , and for each  $x$  there are  $2^{n-m}$  unspecified bit values so  $|\mathcal{V}_x| = 2^{n-m}$ . To implement  $m'$  single-qubit measurements, simply set  $m = 1$  and repeat  $m'$  times. This exponential growth in the spatial extent of the required measurement operators is why previous quantum-walk models have been proposed primarily in terms of computational capability, and not in terms of possible physical implementations. It also makes the prospect of implementing quantum error correcting codes impractical at best.

In contrast, the Bose–Hubbard-based multi-walker model presented here allows for the measurement of  $m$  qubits with localized measurement operators. Define

$$P_{i,x}^{(b)} = (\hat{c}_{i,x}^\dagger)^b |0_{i,x}\rangle\langle 0_{i,x}| (\hat{c}_{i,x})^b = |b_{i,x}\rangle\langle b_{i,x}|, \quad (29)$$

the projector onto the state with exactly  $b$  walkers on vertex  $v_{i,x}$ . The qubit encoded on vertices  $v_{i,0}$  and  $v_{i,1}$  can then be measured with the operators

$$M_{i,0} = P_{i,0}^{(1)} \otimes P_{i,1}^{(0)} \otimes I_{\bar{i}}, \quad (30a)$$

$$M_{i,1} = P_{i,0}^{(0)} \otimes P_{i,1}^{(1)} \otimes I_{\bar{i}}, \quad (30b)$$

where  $I_{\bar{i}}$  is the identity operator on every vertex not labeled by  $i$ . These two operators form a measurement basis for the system since the allowed states when a measurement is to be performed have at most one walker on vertex  $v_{i,x}$ , so the identity operator on that vertex can be resolved as

$$I_{i,x} = |0_{i,x}\rangle\langle 0_{i,x}| + |1_{i,x}\rangle\langle 1_{i,x}| = P_{i,x}^{(0)} + P_{i,x}^{(1)}. \quad (31)$$

Furthermore the probability to find either zero or two (or more) walkers on the pair of vertices  $\{v_{i,0}, v_{i,1}\}$  vanishes, so all other two-site projectors

$$P_{i,0}^{(a)} \otimes P_{i,1}^{(b)}, \quad a + b \neq 1, \quad (32)$$

are not part of the basis for the states encoding qubit  $i$ .

As in the single-walker case we can perform a single-qubit measurement with one pair of measurement operators, but in this case each operator is spatially localized to two vertices regardless of  $n$ . Performing an  $m$ -qubit measurement in a single step, as opposed to by making  $m$  single-qubit measurements in succession, requires a set of  $2^m$  measurement operators of the form (30). Again, each one requires projectors only onto single vertices.

With the ability to perform single-qubit measurements on the multi-walker system in a straightforward manner comes the ability to implement those quantum error

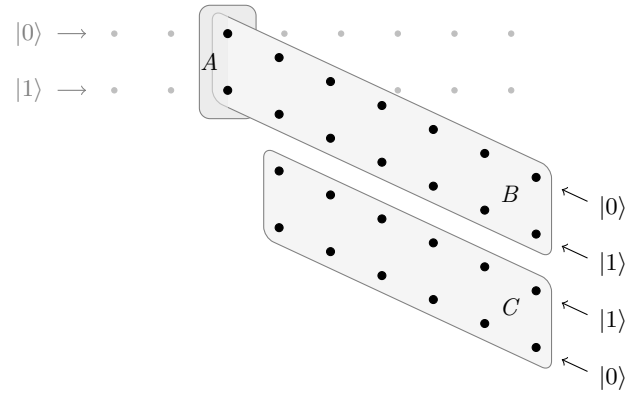


FIG. 7. Addition of the seven-qubit Steane quantum error-correcting code to the Bose–Hubbard-based multi-walker scheme for universal quantum computation. The computation scheme described in Sec. II takes place on the horizontal row of light-gray vertices, in which the two in region  $A$  have been singled out as the qubit to be encoded in this cartoon. The 14 vertices of region  $B$  (including those in  $A$ ) provide seven physical qubits with which to encode a single logical qubit. Region  $C$  provides six additional ancillary qubits that can be entangled with those of the logical qubit in order to perform syndrome measurements as a sequence of single-qubit measurements. Note that the ordering of the  $|0\rangle$  and  $|1\rangle$  rows has been reversed in  $C$  with respect to  $B$ ; this allows a straightforward method of generating entanglement between the two regions by way of the CPHASE gate that results from an edge between the  $|1\rangle$  vertices of neighboring qubits.

correcting codes (QECCs) that rely on encoding a single logical qubit in multiple physical ones [24–26]. One such code is the seven-qubit Steane code [27], a so-called CSS code capable of detecting and correcting arbitrary single-qubit errors and of being implemented fault tolerantly since operations on encoded logical qubits can be implemented by way of local operations on the underlying physical qubits. This and other QECCs can be implemented directly within the multi-walker framework already discussed in previous sections, constructing the requisite operators to within a desired error tolerance from a polynomial number of gates from the universal set provided. An alternative, which we now discuss for the seven-qubit Steane code in particular, is to use a straightforward extension of the qubit-encoding scheme. Consider extending the  $2 \times n$  grid into the third dimension, to a  $2 \times 7 \times n$  array of vertices or, when it is easier to perform syndrome measurements as single-qubit measurements rather than the four-qubit measurement operators described by the code, to  $4 \times 7 \times n$ , as depicted in Fig. 7. Each pair of vertices encoding a single qubit in the original scheme described above, as in Region  $A$  of Fig. 7, has a further six pairs extending from it along the third dimension of the lattice. The resulting total of seven pairs at a given position  $i$  within the lattice, Region  $B$ , allows for the creation of a single logical qubit. Six further ancillary qubits, Region  $C$ , can be entangled with the physical qubits of the logical one

in order to implement syndrome measurements on single qubits. Making the vertices that correspond to the  $|1\rangle$  states in the two regions adjacent allows entanglement to be generated between them by the CPHASE gate (22) with the straightforward addition of edges between the logical region and the ancillary one.

Logical operations on these additional qubits can of course be performed in exactly the same manner as on the original qubits described in Sec. II. Those gates are dependent on certain couplings between pairs of vertices, but are not inherently reliant on a grid- or lattice-like structure in the placement of those vertices; such a setting merely provides a useful visualization method, and yields an obvious tie to possible extant physical systems as we discuss in Sec. IV. They can therefore all be applied between pairs of qubits in this new arrangement as well.

Having seen that our multi-walker Bose–Hubbard-based approach to universal computation provides the advantage of being able to implement computational error correction, previously unaddressed within quantum walk-based quantum computation, we also note that the dynamical nature of the underlying graph introduces a second potential source of error. If a gate is timed incorrectly, it is possible for the system to end up in a physical state that does not encode a computational one – besides being flipped and dephased, a qubit can be lost altogether. When this possibility is allowed for, the measurement operators (30) no longer sum to the identity and we must introduce a third operator,

$$M_{i,\text{err}} = I - M_{i,0} - M_{i,1}. \quad (33)$$

This provides a simple method for detecting the loss of a qubit, but not a mechanism for recovering from it. The possibility of losing the walker exists in the original proposal for universal quantum computation by a single quantum walker [12], and a similar timing issue is present in the discontinuous-walk scheme [14] as well as any potential physical scheme for the simulation of a discrete-time quantum walk with a continuously evolving physical system. These are not fundamental limitations on quantum walk-based computing, but must be considered in any serious attempt to engineer such systems.

#### IV. PHYSICAL IMPLEMENTATION

A key feature required of a physical system that is to implement this proposal is the ability to provide the specified  $2 \times n$  lattice — or three-dimensional lattice, if that method of implementing a QECC is chosen — such that the tunneling amplitude between neighboring sites is close to zero when no gate is being enacted. This corresponds to the qubits’ having a long coherence time. In practice this can be accomplished in either the 2D or 3D case by creating a three-dimensional lattice with isolated wells, and ignoring any vertices outside of the primary graph to be implemented.

The additional requirements of state preparation, manipulation, and read-out are common to any quantum computer [28], and we discuss them here in the context of our proposal. State preparation is accomplished by the initialization of the  $|0\rangle^{\otimes n}$  state, by loading one boson onto the first of each pair of sites in the primary graph. To manipulate the encoded qubits, it must be possible to selectively increase the tunneling amplitude between given adjacent sites in order to enact  $X$ , CPHASE, and SWAP gates, and to change on-site potentials to enact  $Z$  gates. Finally to read out the result of a computation it must be possible to measure the positions of the bosonic walkers within the lattice, as discussed in Sec. III.

The experimental scheme proposed in Ref. [23] includes many of the features required, though it makes use of adiabatic processes for gate executions. A combination of this approach with the sudden potential-landscape changes discussed in Ref. [29] is more appropriate to the current scheme, and there have been significant experimental advances in the intervening years that offer the promise of a proof-of-principle implementation.

There is an obvious connection between our scheme and optical-lattice experiments, and several experiments satisfy the above requirements. One option is to use a liquid-crystal display (LCD) as a spatial light modulator [30]. Such devices generate arrays of microtraps holographically based on the pattern of opacity and transparency present on the easily programmed LCD screen. The traps have been used to store single neutral atoms per site, address individual sites, and measure the locations of trapped atoms within the lattice [30], thus providing a means to create the primary graph as well as implement preparation, manipulation, and read-out.

Another possibility is to combine a set of recently demonstrated experimental capabilities. Wide lattice spacings on the order of  $5\ \mu\text{m}$  have been achieved [31], providing a long coherence time to the sites and effectively approximating the infinitely deep lattice of the primary graph. A quantum gas microscope, employing a high-numerical-aperture lens, has been used to image individual sites in a traditional optical lattice [32]. Repurposing such a system to focus a laser to a similar resolution would provide a method of manipulating qubits by addressing single sites in the case of a  $Z$  gate, or modifying the potential between sites in the case of  $X$  and CPHASE gates. Most recently, arbitrary configurations of atom positions within a lattice have been implemented [33], which in particular would allow for the straightforward preparation of the initial  $|0\rangle^{\otimes n}$  state as a single straight line, one atom wide. In each of these experiments, read-out of the positions of the trapped atoms is also performed.

#### V. CONCLUSIONS

The Bose–Hubbard model, a well-known and widely applicable description of bosons confined to a lattice, can



be used to generate a universal set of quantum logic gates. These gates act on quantum information encoded in the positional states of spinless bosons, in contrast to the standard method of using internal degrees of freedom to store information. Despite arising from Hamiltonians that couple outside of the computational space, the gates are nevertheless unitary when the evolution parameters are tuned appropriately. The concept of encoding a computational space as a subspace of a larger physical Hilbert space is often considered to be detrimental or artificial when couplings are present between the subspace and the larger space. We have shown that such a system can gain power from its ability to access that larger space during evolution, while nevertheless remaining restricted to the computational subspace by the end of its evolution.

Bosons hopping on a lattice under the Bose–Hubbard model can also be interpreted as multiple interacting quantum walkers on a primary graph that encodes the sites and tunneling amplitudes of the lattice in its vertices and edges, respectively. The use of multiple quantum walkers allows for a sequence of graphs on  $O(n)$  vertices to encode a quantum computation on  $n$  qubits by dis-

continuous walk. Such a setup can also be interpreted as a single quantum walker on a graph with  $\Omega(2^n)$  vertices and connected to the standard rail model for computation by quantum walk, showing the power of multiple walkers to eliminate the need for exponentially growing resources. Furthermore, localized single-qubit measurement operators are now possible in a quantum-walk scenario, and we have presented one example of a scheme to implement quantum error-correcting codes with multiple quantum walkers under the Bose–Hubbard model.

Finally, we have discussed the possibility of adapting current experimental methods to implement a proof-of-principle version of our proposal. Trapped neutral atoms in optical lattices with various methods for addressing individual sites and manipulating the potential landscape fulfill the requirements of such an implementation.

## ACKNOWLEDGMENTS

This work was supported by the Natural Sciences and Engineering Research Council of Canada (NSERC) and by Alberta Innovates Technology Futures.

- 
- [1] J. Kempe, *Contemp. Phys.* **44**, 307 (2003).
  - [2] A. Ambainis, *Int. J. Quant. Inf.* **1**, 507 (2003).
  - [3] A. Ambainis, A. M. Childs, B. W. Reichardt, R. Špalek, and S. Zhang, in *48th Annual IEEE Symposium on Foundations of Computer Science (FOCS 2007)* (2007), pp. 363–372.
  - [4] A. M. Childs, R. Cleve, E. Deotto, E. Farhi, S. Gutmann, and D. A. Spielman, in *Proceedings of the 35th annual ACM symposium on Theory of computing (STOC 2003)* (ACM, New York, 2003), pp. 59–68.
  - [5] A. M. Childs, R. Cleve, S. P. Jordan, and D. Yonge-Mallo, *Theor. Comput.* **5**, 119 (2009).
  - [6] R. Cleve, D. Gavinsky, and D. Yonge-Mallo, in *Theory of Quantum Computation, Communication, and Cryptography*, edited by Y. Kawano and M. Mosca (Springer Berlin / Heidelberg, 2008), vol. 5106 of *Lecture Notes in Computer Science*, pp. 11–15, ISBN 978-3-540-89303-5.
  - [7] E. Farhi, J. Goldstone, and S. Gutmann, *Theor. Comput.* **4**, 169 (2008).
  - [8] B. Reichardt and R. Špalek, in *Proceedings of the 40th annual ACM symposium on Theory of computing (STOC 2008)* (2008), pp. 103–112.
  - [9] M. Santha, in *Theory and Applications of Models of Computation*, edited by M. Agrawal, D. Du, Z. Duan, and A. Li (Springer Berlin / Heidelberg, 2008), vol. 4978 of *Lecture Notes in Computer Science*, pp. 31–46, ISBN 978-3-540-79227-7.
  - [10] F. Magniez, M. Santha, and M. Szegedy, in *Proceedings of the sixteenth annual ACM-SIAM symposium on Discrete algorithms* (Society for Industrial and Applied Mathematics, Philadelphia, PA, USA, 2005), SODA '05, pp. 1109–1117, ISBN 0-89871-585-7.
  - [11] A. Ambainis, *SIAM J. Comput.* **37**, 210 (2007).
  - [12] A. M. Childs, *Phys. Rev. Lett.* **102**, 180501 (2009).
  - [13] N. B. Lovett, S. Cooper, M. Everitt, M. Trevers, and V. Kendon, *Phys. Rev. A* **81**, 042330 (2010).
  - [14] M. S. Underwood and D. L. Feder, *Phys. Rev. A* **82**, 042304 (2010).
  - [15] P. P. Rohde, A. Schreiber, M. Štefaňák, I. Jex, and C. Silberhorn, *New J. Phys.* **13**, 013001 (2011).
  - [16] P. Xue and B. C. Sanders, *Phys. Rev. A* **85**, 022307 (2012).
  - [17] I. Carneiro, M. Loo, X. Xu, M. Girerd, V. Kendon, and P. L. Knight, *New J. Phys.* **7**, 156 (2005).
  - [18] J. K. Gamble, M. Friesen, D. Zhou, R. Joynt, and S. N. Coppersmith, *Phys. Rev. A* **81**, 052313 (2010).
  - [19] M. P. A. Fisher, P. B. Weichman, G. Grinstein, and D. S. Fisher, *Phys. Rev. B* **40**, 546 (1989).
  - [20] O. Romero-Isart, K. Eckert, C. Rodó, and A. Sanpera, *J. Phys. A: Math. Theor.* **40**, 8019 (2007).
  - [21] C. Bruder, R. Fazio, and G. Schön, *Ann. der Physik* **14**, 566 (2005).
  - [22] M. Greiner, O. Mandel, T. Esslinger, T. W. Hänsch, and I. Bloch, *Nature* **415**, 39 (2002).
  - [23] J. Mompart, K. Eckert, W. Ertmer, G. Birkl, and M. Lewenstein, *Phys. Rev. Lett.* **90**, 147901 (2003).
  - [24] P. W. Shor, *Phys. Rev. A* **52**, R2493 (1995).
  - [25] A. R. Calderbank and P. W. Shor, *Phys. Rev. A* **54**, 1098 (1996).
  - [26] R. Laflamme, C. Miquel, J. P. Paz, and W. H. Zurek, *Phys. Rev. Lett.* **77**, 198 (1996).
  - [27] A. Steane, *Proc. R. Soc. Lond. A* **452**, 2551 (1996).
  - [28] D. P. DiVincenzo, in *Mesoscopic Electron Transport*, edited by L. L. Sohn, L. P. Kouwenhoven, and G. Schön (Kluwer Academic Publishers, 1997), vol. 345 of *NATO Advanced Study Institute, Series E: Applied Sciences*.
  - [29] T. Calarco, E. A. Hinds, D. Jaksch, J. Schmiedmayer, J. I. Cirac, and P. Zoller, *Phys. Rev. A* **61**, 022304 (2000).

- [30] S. Bergamini, B. Darquié, M. Jones, L. Jacubowicz, A. Browaeys, and P. Grangier, *J. Opt. Soc. Am. B* **21**, 1889 (2004).
- [31] K. D. Nelson, X. Li, and D. S. Weiss, *Nature Physics* **3**, 556 (2007).
- [32] W. S. Bakr, J. I. Gillen, A. Peng, S. Fölling, and M. Greiner, *Nature* **462**, 74 (2009).
- [33] C. Weitenberg, M. Endres, J. F. Sherson, M. Cheneau, P. Schauß, T. Fukuhara, I. Bloch, and S. Kuhr, *Nature* **471**, 319 (2011).